DOI: 10.1002/ejic.201100347

Complex Intermetallic Compounds: $CaNi_5Ge_3$, $Ca_{15}Ni_{68}Ge_{37}$, and $Ca_7Ni_{49}Ge_{22}$ – Three Multifaceted Ni-Ge Framework Structures Combining the Structural Motifs of Ni_3Ge and $CaNi_2Ge_2$

Lisa Siggelkow,[a] Viktor Hlukhyy,[a] Bernhard Wahl,[a] and Thomas F. Fässler*[a]

Dedicated to Professor John D. Corbett on the occasion of his 85th birthday

Keywords: Intermetallic phases / Alloys / Germanides / Electron Localization Function / Structure elucidation

The intermetallic compounds, $CaNi_5Ge_3$, $Ca_{15}Ni_{68}Ge_{37}$, and $Ca_7Ni_{48.9(4)}Ge_{22.1(4)}$, were prepared by arc-melting of the elements and subsequent heating in welded tantalum ampoules. The compounds were investigated by powder and single-crystal X-ray diffraction methods. Each of the three compounds crystallized in a different structure type, namely, $CaNi_5Ge_3$ in the space group $P4/mbm$, a = 8.0855(1) Å, c = 7.8466(1) Å, wR_2 = 0.054, 439 F^2 values, 31 variable parameters; $Ca_{15}Ni_{68}Ge_{37}$ in the space group $P\bar{6}2m$, a = 22.436(2) Å, c = 3.9684(4) Å, wR_2 = 0.096, 1849 F^2 values, 133 variable parameters; $Ca_7Ni_{48.9(4)}Ge_{22.1(4)}$ in the space group $P6/mmm$, a = 17.381(4) Å, c = 4.046(1) Å, wR_2 = 0.082, 693 F^2 values, 59 variable parameters. The crystal structures consist of complex 3D networks of nickel and germanium atoms that have common motifs, namely, different sections of the Ni_3Ge structure, as well as, Ca-centered hexagonal prisms of Ni and Ge, which have been observed in the $CaNi_2Ge_2$ structure. As the Ca content decreases, the Ni-Ge substructures form one-, two-, and three-dimensional networks. The disorder in $Ca_7Ni_{48.9(4)}Ge_{22.1(4)}$ is explained by a structural frustration. The electronic structure and chemical bonding of $CaNi_5Ge_3$ is discussed by means of band-structure calculations.

Introduction

During the last decades the structural investigations of the binary and ternary pnictides, with a metal to nonmetal ratio equal to or close to two, has attracted a lot of interest. For example, in the series with the general formula $R_{n(n-1)}T_{(n+1)(n+2)}P_{n(n+1)+1}$ (R = Zr or rare earth metal, T = 3d or 4d transition metal, n = 1 to 6), Fe_2P (n = 0),[1] $Zr_2Fe_{12}P_7$ (n = 2),[2] $Zr_6Ni_{20}P_{13}$ (n = 3),[3] $(La,Ce)_{12}Rh_{30}P_{21}$ (n = 4),[4] $Sm_{20}Ni_{42}P_{31}$ (n = 5), and $Tb_{30}Ni_{56}P_{43}$ (n = 6)[5] have been described thoroughly.[6–8] The corresponding arsenides with n = 4 ($Dy_{12}Ni_{30}As_{21}$ and $Tb_{12}Ni_{30}As_{21}$)[9] and n = 5 [$R_{20}Ni_{42}As_{31}$ (R = La, Ce, Pr, Nd, Sm)][10] have also been reported. The outstanding structural motif of these structures contains rods of condensed hexagonal prisms $^1{}_\infty[R(T_{3/1}X_{3/1})_{2/2}]$ with R in the center, which are linked by means of the rectangular faces to form triangular units of 1, 3, 6, 10, and 15 hexagonal prisms. In this context, the structurally similar series $R_{n(n+1)}T_{6(n^2+1)}Si_{2(2n^2+1)}$, and its representatives $U_6Co_{30}Si_{18}$ (UCo_5Si_3) (n = 2),[11] $U_{12}Co_{60}Si_{38}$ (n = 3),[12] and $U_{20}Co_{102}Si_{66}$ (n = 4),[13] which also contain condensed, R-centered $^1{}_\infty[R(T_{3/1}X_{3/1})_{2/2}]$ hexagonal prisms, should be mentioned. Here, the hexagonal prisms are both vertex- and face-linked and also form triangular units. Furthermore, some indides of the systems R/T/In (R = Ca, Sr, Eu; T = Au, Pt), which contain capped hexagonal prisms as coordination polyhedra of R, have been reported.[14–16] The comparatively small and constant c axis (about 3.7 Å) is common to all of the structure types and corresponds to the height of a hexagonal prism. In contrast, the a and b axes increase with the complexity of the linkage of the hexagonal prisms.

While such hexagonal structures are quite common for P, As, and In, for the group 14 elements these structural motifs have mainly been described for Si.[11–13,17] For Ge, some structures that resemble the hexagonal structures mentioned above are known: $CePt_7Ge_4$ contains Pt_6Ge_6 and Pt_8Ge_4 hexagonal prisms that have Ce at the center.[18] In $Ln_3Pt_4Ge_6$ (Ln = Ce, Pr–Dy)[19,20] and $Y_3Pt_4Ge_6$[21] the Ln/Y coordination polyhedra are pentagonal and hexagonal prisms.

In the course of our investigations of the Ca/Ni/Ge system several ternary compounds, which contain two-dimensional Ni-Ge layers (CaNiGe, $Ca_4Ni_4Ge_3$, $Ca_2Ni_3Ge_2$)[22–24] as well as three-dimensional Ni-Ge networks ($CaNi_2Ge_2$, $CaNiGe_3$, $CaNiGe_2$)[25–27], have been characterized. Further research led to the discovery of the title compounds $CaNi_5Ge_3$, $Ca_{15}Ni_{68}Ge_{37}$, and $Ca_7Ni_{48.9(4)}Ge_{22.1(4)}$, each of

[a] Department Chemie, Technische Universität München, Lichtenbergstr. 4, 85747 Garching, Germany
E-mail: thomas.faessler@lrz.tu-muenchen.de

Supporting information for this article is available on the WWW under http://dx.doi.org/10.1002/ejic.201100347.

which crystallized in a new structure type. The crystal structure of $CaNi_5Ge_3$ can be described as a combination of the structural motifs of $CaNi_2Ge_2$ ($ThCr_2Si_2$ structure type)[28] and Ni_3Ge[29] ($AuCu_3$ structure type)[30]. Both of the motifs are also found in the two further title compounds, $Ca_{15}Ni_{68}Ge_{37}$ and $Ca_7Ni_{48.9(4)}Ge_{22.1(4)}$. The resulting building blocks, namely, the Ca-centered condensed hexagonal prisms of the Ni and Ge atoms, can be discussed in the context of the structures mentioned above. The synthesis, the description of the crystal structures of the title compounds, as well as the electronic structure and the magnetic properties of $CaNi_5Ge_3$, are discussed in this article.

Results and Discussion

The synthesis of the ternary title compounds was achieved by a two-step arc-melting procedure that formed at first a Ni-Ge alloy. This step was followed by the arc-melting of this alloy with elemental Ca. A variation of the stoichiometry resulted in the formation of three new intermetallic compounds. The structures and compositions of the compounds $CaNi_5Ge_3$, $Ca_{15}Ni_{68}Ge_{37}$, and $Ca_7Ni_{48.9(4)}Ge_{22.1(4)}$ were determined by single-crystal X-ray diffraction methods. In all cases the differentiation of the elements, with relatively similar valence electrons to Ge and Ni, is undoubtedly possible. In $CaNi_5Ge_3$ and $Ca_{15}Ni_{68}Ge_{37}$ no disorder is observed. $Ca_7Ni_{48.9(4)}Ge_{22.1(4)}$, however, showed a mixed occupancy of Ni and Ge on one specific site. Compared to the other intermetallic compounds known in the Ca/Ni/Ge system, the title phases $CaNi_5Ge_3$, $CaNi_{4.53}Ge_{2.47}$, and $CaNi_7Ge_{3.14}$ are Ni rich and are composed of closely related structural building motifs.

The crystal structures of $CaNi_5Ge_3$, $Ca_{15}Ni_{68}Ge_{37}$, and $Ca_7Ni_{48.9(4)}Ge_{22.1(4)}$ consist of complex three-dimensional networks that are built of the Ni and Ge atoms. Parts of the Ni-Ge substructures represent low-dimensional cutouts of the Ni_3Ge structure, which are separated by the Ca atoms. The coordination polyhedra of the Ca atoms are condensed hexagonal prisms of Ni and Ge atoms, which are common structure motifs.

An overview of the three title compounds is given in Figure 1. In $CaNi_5Ge_3$, two-dimensional Ni-Ge layers (which can be deduced from the Ni_3Ge structure as will be shown below) that are parallel to the *bc* plane are separated by Ca atoms (Figure 1, a). In the Ca-richer compound, $Ca_{15}Ni_{68}Ge_{37}$, (Figure 1, b) ribbons of these Ni-Ge layers are arranged at a 60° angle to form triangular units. These units enclose six parallel condensed rods of Ca-centered hexagonal Ni-Ge prisms. In addition, these trigonal units are separated from each other by a network of further condensed Ca-centered hexagonal Ni-Ge prisms. Finally, in the Ca-poorest compound, $Ca_7Ni_{48.9(4)}Ge_{22.1(4)}$, (Figure 1, c) similar segments of the above mentioned Ni-Ge layers are arranged at a 60° angle. In this case, a three-dimensional Ni-Ge network, which is clasped around the rods of condensed Ca-centered hexagonal Ni-Ge prisms, results.

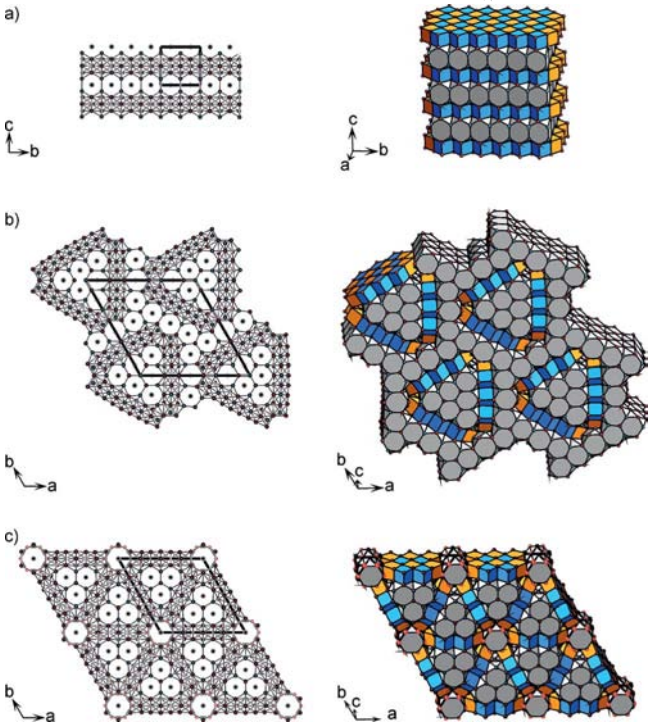

Figure 1. Two views of the crystal structures of (a) $CaNi_5Ge_3$, (b) $Ca_{15}Ni_{68}Ge_{37}$, and (c) $Ca_7Ni_{48.9(4)}Ge_{22.1(4)}$. Left-hand side: Projection along the *a* axis ($CaNi_5Ge_3$) and along the *c* axis ($Ca_{15}Ni_{68}Ge_{37}$ and $Ca_7Ni_{48.9(4)}Ge_{22.1(4)}$), which emphasizes the Ni-Ge slabs and the Ni-Ge channels that are filled with Ca. The Ca atoms are at the center of the face-sharing condensed hexagonal prisms. The chosen Ni–Ge bonds emphasize the different structural motifs. The Ca atoms are drawn as black spheres and the Ge and Ni atoms are drawn as blue and red ones, respectively. The coordination polyhedra of Ca are drawn in grey. The Ge- and Ni-centered distorted cubes are drawn in blue and orange, respectively. The mixed position, Ge1/Ni1, is given as a blue sphere with red borderlines.

The unit cell parameter *c* for $Ca_{15}Ni_{68}Ge_{37}$ and $Ca_7Ni_{48.9(4)}Ge_{22.1(4)}$ is about 4 Å, which is similar to that of *c* for the pnictides and silicides described in the introduction, and corresponds to the height of a hexagonal prism. The corresponding parameter *a* (or *b*) for $CaNi_5Ge_3$ is doubled due to a weak distortion. The other unit cell parameters vary depending on the combination of the structural motifs. Consequently, the prominent structural motifs of the hexagonal structures ($Ca_{15}Ni_{68}Ge_{37}$ and $Ca_7Ni_{48.9(4)}Ge_{22.1(4)}$) are observed in a projection along the *c* axis and along the *a* (or *b*) axis for the tetragonal compound, $CaNi_5Ge_3$.

Crystal Structure of $CaNi_5Ge_3$

The compound $CaNi_5Ge_3$ crystallizes with a new structure type, which was determined from the single-crystal X-ray diffraction data: *P4/mbm*, $Z = 4$, $a = 8.0855(1)$ Å, $c = 7.8466(1)$ Å, $wR_2 = 0.054$.

A schematic view of the structure of $CaNi_5Ge_3$ (Figure 2, d–g), together with the structures of Ni_3Ge (Figure 2, a and b) and $CaNi_2Ge$ (Figure 2, c), is given in Figure 2. For the

cubic Ni_3Ge structure, two perspectives are given in order to enable a further comparison to the title compounds: in Figure 2 (a) a slab of the Ni_3Ge structure, which is represented as elongated Ge- and Ni-centered cuboids with Ni atoms on the vertices, is shown. Furthermore, the coordination polyhedra of Ge and Ni (regular cuboctahedra) are shown once. When these elongated Ge- and Ni-centered cuboids are focussed on, two parallel, congruent square layers of Ni atoms appear as the predominant feature (Figure 2, b). Between these square layers of Ni atoms, a further square layer of alternating Ni and Ge atoms is inserted. Thus, the resulting Ni cuboids have alternating Ni and Ge atoms at the center. Note that the compression of these cuboids leads to a primitive cubic lattice with cubes that have alternating Ge and Ni atoms at the center. Thus, the ordered Fe_3Al structure type[31] is obtained.

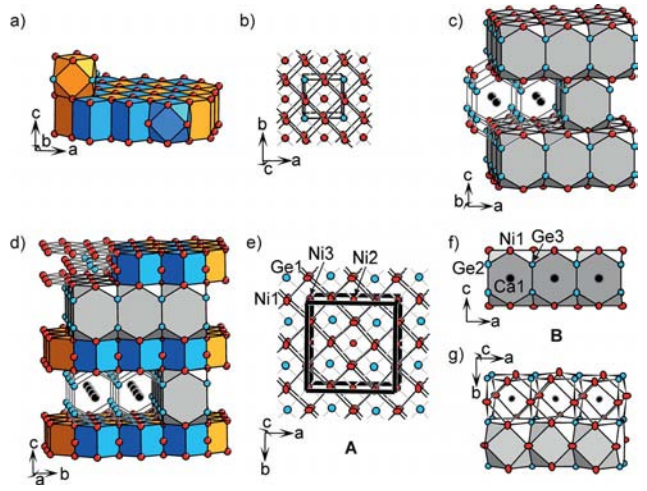

Figure 2. The relationship between the crystal structures of Ni_3Ge [(a) and (b)], $CaNi_2Ge_2$ [(c)], and $CaNi_5Ge_3$ [(d) to (g)]. (a) A two-dimensional section of the Ni_3Ge structure, (b) a two-dimensional section of the Ni_3Ge structure shown along the *c* axis, (c) condensed Ca-centered Ni_4Ge_8 hexagonal prisms of $CaNi_2Ge_2$, (d) crystal structure of $CaNi_5Ge_3$, the structure motifs **A** and **B** are emphasized, (e) a layer of Ni_3Ge in $CaNi_5Ge_3$ (building block **A**), (f) and (g) the structural motif **B** with the Ca-centered hexagonal prisms along the *b* axis and the *c* axis. The Ca atoms are drawn as black spheres and the Ge and Ni atoms are drawn as blue and red ones, respectively. The coordination polyhedra of Ca are drawn in grey. The Ge- and Ni-centered distorted cubes are drawn in blue and orange, respectively. The displacement ellipsoids in (e) to (g) are drawn at the 95% probability level.

The title compound can be interpreted as an intergrowth of building block **A** (Figure 2, e), which can be deduced from the Ni_3Ge structure, and the structural motif **B** (Figure 2, f and g) of the $CaNi_2Ge_2$ structure with an **ABAB** stacking sequence along the *c* axis.

In Figure 2 (e) the substructure **A** of $CaNi_5Ge_3$, which has the composition $^2_\infty[Ni_3Ge]$, is given; the viewing direction is parallel to the *c* axis. The Ni1 atoms form distorted square layers that are situated parallel to the *ab* plane. A further distorted square layer of Ge1, Ni2, and Ni3 atoms is inserted between these two Ni1 layers. The resulting coordination polyhedra of the Ni2 and Ni3 atoms are distorted cubes that consists of Ni atoms (Ni1) and are capped by six Ge atoms (four Ge1 atoms are at the center of the neighbouring distorted cubes and two Ge2 and Ge3 atoms, which belong to building block **B**). The coordination polyhedron of Ge1 is a distorted cuboctahedron, which consists of a distorted cube of Ni atoms (Ni1) that is capped by four further Ni atoms (Ni2, Ni3). The latter are at the center of the neighbouring distorted cubes. In the cubic Ni_3Ge the shortest Ni–Ge and Ni–Ni distances are both d = 2.52 Å (distance between the centering atoms and the vertices of the cuboids as well as the distances within the square Ni layers and within the square Ni-Ge layers). The interlayer distance between the atoms of the two square Ni layers (3.57 Å) corresponds to the next-nearest-neighbour interactions. In comparison, the cuboids in $CaNi_5Ge_3$ are compressed: the shortest distances are found between the centering atoms of the distorted cubes and the corresponding vertices [from d(Ge1–Ni1) = 2.458(1) Å to d(Ni2–Ni1) = 2.477(1) Å]. The distances between the centering atoms (i.e., between Ge1, Ni2, Ni3) are significantly larger [from d(Ge1–Ni2) = 2.707(1) Å to d(Ge1–Ni2) = 3.010(1) Å]. In comparison to Ni_3Ge, the distances between the distorted square layers of the Ni1 atoms are shorter [d(Ni1–Ni1) = 2.822(2) Å].

The coordination polyhedron around Ca, which is labelled with **B** (Figures 2, f and g), is similar to the Ca polyhedron in $CaNi_2Ge_2$ (Figure 2, c). This 16-vertex coordination polyhedron of Ca is formed by eight Ni (8× Ni1) and eight Ge atoms (4× Ge2, 4× Ge3), and can be regarded as a hexagonal prism with four rectangular faces that are capped by Ni1 atoms. These $Ca@Ni_8Ge_8$ polyhedra are condensed in two dimensions via the Ni_2Ge_4 hexagonal faces, which each contain two direct Ge–Ge bonds. The resulting structure unit layers can be described by the Niggli formula, $^2_\infty[Ca(Ni_{2/1}Ge_{4/2})_{2/2}Ni_{4/2}]$.[32] As shown in Figure 2 (c), the stacking of these layers in the *c* direction leads to the $CaNi_2Ge_2$ structure. In contrast, in $CaNi_5Ge_3$ a layer of the Ni_3Ge structure type (**A**) is inserted between these layers (**B**). The interatomic distances in $CaNi_2Ge_2$ and $CaNi_5Ge_3$ are rather similar (Table 3): in $CaNi_2Ge_2$ the Ge–Ge distance (2.60 Å) is slightly longer than that in $CaNi_5Ge_3$ [2.551(3) Å] and the Ni–Ge distances are approximately equal [$CaNi_2Ge_2$: d(Ni–Ge) = 2.36 Å; $CaNi_5Ge_3$: d(Ni1–Ge2) = 2.369(2) Å, d(Ni1–Ge3) = 2.363(2) Å]. Due to the distortion of the square layer of Ni1 atoms, the Ni–Ni distances in $CaNi_5Ge_3$ [d(Ni1–Ni1) = 2.707(2) Å to d(Ni1–Ni1) = 3.042(2) Å] vary around those in $CaNi_2Ge_2$ [d(Ni–Ni) = 2.88 Å]. In $CaNi_5Ge_3$ the structural motif **A** alternates with the building block **B**. However, the substructure of **A** also plays a key role in the two further title compounds.

A further possible description of the $CaNi_5Ge_3$ structure consists of the examination of the planar atom layers that are aligned parallel to the *ac* plane (Figure 3). The layer α is located at y = 0 and 1/2 (Figure 3, b); the layer β appears at y = 1/4 (Figure 3, c) and the layer β′ (equivalent to β) at y = 3/4. The resulting stacking sequence is αβαβ′. β and β′ are identical layers, however, β′ is shifted slightly along the *a* axis in comparison to β. For the sake of clarity in Figure 3

the layers α and β are shown without interlayer contacts. The composition of the layers α and β (or β′) are "Ni_6Ge_4" and "$Ca_2Ni_4Ge_2$", respectively. It is worth noting that the layer α contains exclusively Ni and Ge atoms, while Ca atoms are situated within the β (or β′) layers.

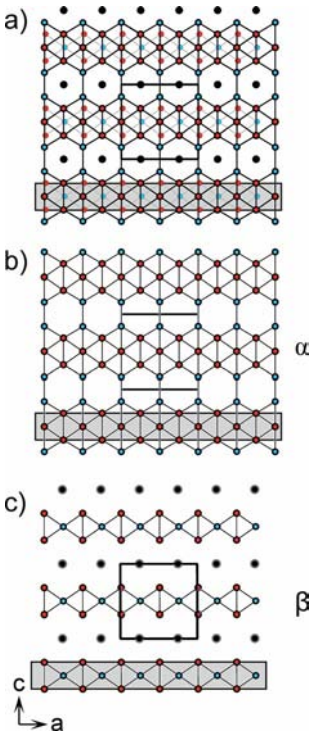

Figure 3. (a) The crystal structure of $CaNi_5Ge_3$. The two layers, (b) α at $y = 0$ and (c) β at $y = ¼$, are given. The sections that are deduced from the Ni_3Ge structure type are highlighted in grey. The Ca atoms are drawn as black spheres and the Ge and Ni atoms are drawn as blue and red ones, respectively.

A very similar structure has been observed recently for UFe_5Si_3.[33] The symmetry and the atom arrangement are close to $CaNi_5Ge_3$, however, due to a weak distortion in $CaNi_5Ge_3$, the unit cell is doubled along the *a* and *b* axes. As the structure of UFe_5Si_3 was determined by means of ab initio Rietveld refinement from powder X-ray diffraction data, the possibility that both compounds crystallize in the same "distorted" structure type cannot be ruled out. Furthermore, the structure of $CaNi_5Ge_3$ is closely related to the Zintl phase, $BaMg_4Ge_3$,[34] and may be regarded as its filled variant. The Ba atoms are replaced by Ca and the Mg atoms are replaced by Ni. The atomic positions of Ni2 and Ni3 in the title phase are vacant in $BaMg_4Ge_3$. Due to the weak distortion of $CaNi_5Ge_3$, the *a* and *b* parameters are doubled.

Crystal Structure of $Ca_{15}Ni_{68}Ge_{37}$

The compound $Ca_{15}Ni_{68}Ge_{37}$ crystallizes in its own structure type with space group $P\bar{6}2m$ (189) [$Z = 1$, $a = 22.436(2)$ Å, $c = 3.9684(4)$ Å]. The details of the crystal structure for $Ca_{15}Ni_{68}Ge_{37}$ are presented in Figure 4. There are three dominating structural motifs: The Ni-Ge substructure is labeled **A**′ (Figure 4, b), the building block that results from the atoms included in the coordination polyhedra of Ca1 and Ca3 is labeled **B**′ (Figure 4, c), and **C**′ denotes the atoms of the coordination polyhedra of Ca2 and Ca4 (Figure 4, d). The structural motif **A**′ consists of three connected $^1_\infty[Ni_3Ge]$ ribbons that can be derived from the Ni_3Ge structure. In contrast to $CaNi_5Ge_3$, where two-dimensional layers of $^2_\infty[Ni_3Ge]$ are observed, in $Ca_{15}Ni_{68}Ge_{37}$ ribbons of the Ni_3Ge type are connected to a trigonal tube, which run parallel to the *c* axis. These Ni-Ge tubes enclose the structural motif **C**′. This motif **C**′ consists of rods of Ca-centered hexagonal prisms that are condensed by the common hexagonal faces in the *c* direction. In the *ab* plane, six such parallel columns are condensed. The trigonal symmetry is retained along *c* (Figure 4, d). The trigonal Ni-Ge tubes are further separated by the structure motif **B**′ (analogous with **B** in $CaNi_5Ge_3$), which forms a honeycomb structure that encloses the trigonal tubes (Figure 4, c).

The $^1_\infty[Ni_3Ge]$ ribbons of the structural motif **A**′ consist of two ribbons of distorted square layers of Ni atoms (Ni1–6, Ni9, Ni11–13) that result from the outer atom layers of the **B**′ and **C**′ units. A further ribbon of a square layer of alternating Ni and Ge atoms (Ni7, Ni8, Ge1, Ge2, and Ge6) is inserted between these layers. The resulting coordination polyhedra of Ni7, Ni8, Ge2, and Ge6 resembles the ones found in the structural motif **A** of $CaNi_5Ge_3$: The coordination polyhedra of Ge2 and Ge6 are distorted cuboctahedra of Ni atoms and the coordination polyhedra of Ni7 and Ni8 are distorted cubes of Ni atoms that are capped by six Ge atoms. Four edge-sharing distorted cubes, which have Ni atoms (Ni7, Ni8) at the center, determine the width of the ribbons.

As in $CaNi_5Ge_3$, the cuboids are compressed. The distance between the vertices of the distorted cubes and the centering Ge and Ni atoms [*d*(Ge2–Ni1) = 2.372(3) Å to *d*(Ni7–Ni11) = 2.577(3) Å] in the title compound, $Ca_{15}Ni_{68}Ge_{37}$, are significantly shorter than the distances between the centering Ge atoms and the centering Ni atoms [*d*(Ge2–Ni8) = 2.733(2) Å to *d*(Ge2–Ni7) = 2.9845(2) Å] and the distances between the Ni atoms within the distorted square Ni layers [*d*(Ni6–Ni11) = 2.623(2) Å to *d*(Ni1–Ni11) = 3.257(3) Å]. The interlayer distances between the distorted square Ni layers are shorter [*d*(Ni6–Ni11) = 2.618(3) Å to *d*(Ni2–Ni4) = 3.033(5) Å] than those in Ni_3Ge.

The structural motifs **B**′ and **C**′ consist of columns of condensed hexagonal prisms of Ni and Ge atoms, which have Ca atoms at the center. The columns are further connected by means of the rectangular faces of the hexagonal prisms. In **B**′ (Figure 4, c), units of three hexagonal prisms, which are centered by Ca1, form trigonal units. These are further interconnected by the hexagonal prisms that are centered by Ca3. This results in a three-dimensional network with pore-like tubes that are parallel to the *c* axis. The building block **C**′ is situated in these cavities. The vertices of the hexagonal prisms, which are centered by Ca1, are occupied by alternating Ge (Ge4 and Ge5) and Ni (Ni6,

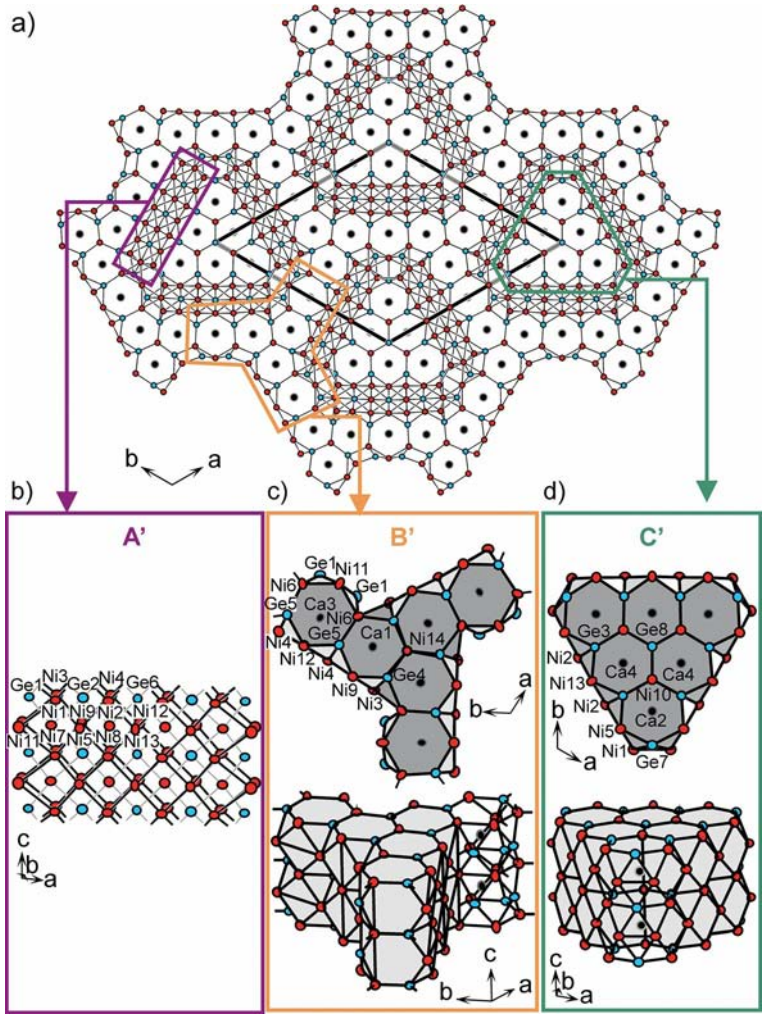

Figure 4. (a) The crystal structure of $Ca_{15}Ni_{68}Ge_{37}$. The different structural motifs are shown in detail: (b) a ribbon of a distorted square layer of Ni7, Ni8, Ge2, and Ge6 that is inserted between two ribbons of Ni square layers (labelled **A′**), (c) the building block that results from the coordination polyhedra of Ca1 and Ca3 (labelled **B′**), and (d) the unit of the coordination polyhedra of Ca2 and Ca4 (labelled **C′**). The Ca atoms are drawn as black spheres and the Ge and Ni atoms are drawn as blue and red ones, respectively. The chosen Ni–Ge bonds emphasize the different structural motifs. The displacement ellipsoids in (b) to (d) are drawn at the 95% probability level.

Ni9, and Ni14) atoms. Ni14 is shared by all three of the hexagons, Ge4 is shared by two of the hexagons. The central unit is fused via common rectangular faces (Ge5 and Ni6) to three further hexagonal prisms, which have Ca3 at the center. These prisms are constructed of hexagons that consist of two Ge atoms (2× Ge5) and four Ni atoms (2× Ni6, Ni11, and Ni12) and can be considered as linkers: they connect the Ca1-centered hexagonal prisms. The Niggli formula of this building block is $^3_\infty[\{Ca(Ni_{1/1}Ni_{1/2}Ge_{3/2}Ni_{1/3})_{2/2}Ni_{3/2}\}_3\{Ca(Ni_{2/1}Ni_{2/2}Ge_{2/2})_{2/2}Ge_{2/1}Ni_{2/2}\}_3]$. The Ni–Ge distances in the building block **B′** of $Ca_{15}Ni_{68}Ge_{37}$ range between *d*(Ge4–Ni14) = 2.338(2) Å and *d*(Ge4–Ni6) = 2.520(3) Å and are comparable to the Ni–Ge distances in other nickel germanides. In contrast, the Ni–Ni distances [from *d*(Ni6–Ni11) = 2.618(3) Å to *d*(Ni3–Ni6) = 3.131(3) Å] are longer than the distances found in *fcc* Ni.

Unit **C′** (Figure 4, d) forms triangular rods and is built of six condensed hexagonal prisms that are centered by Ca4 and Ca2. The inner prisms are centered by Ca4 and the vertices are occupied by alternating Ge (Ge3 and Ge8) and Ni (Ni10 and Ni13) atoms. These prisms are connected by means of the rectangular sides that are built of Ni10 and Ge8 atoms, where the Ge8 is shared by three of the prisms. The hexagonal prisms, which are centered by Ca2, are fused to the inner ones via common rectangular faces (Ni10 and Ge3). The vertices of the Ca2-centered hexagonal prisms are occupied by alternating Ge (Ge3 and Ge7) and Ni (Ni5 and Ni10) atoms. Consequently, Ni10 belongs to three prisms and Ge3 to two prisms. The resulting outer rectangular faces are capped by Ni atoms: the Ni1 atoms cap the rectangular sides that are made up of Ni5 and Ge7, while Ni2 caps two hexagonal prisms above the rectangular sides that are made up of Ni5 and Ge3 as well as Ni13 and Ge3. The resulting triangular rod can be described as $Ca_6@Ge_{20}Ni_{36}$. The Niggli formula of this building block is $^1_\infty[\{Ca(Ni_{1/1}Ge_{2/2}Ni_{2/3}Ge_{1/3})_{2/2}Ni_{2/2}\}_3\{Ca(Ni_{2/1}Ge_{1/1}Ge_{2/2}Ni_{1/3})_{2/2}Ni_{2/1}Ni_{2/2}\}_3]$. The Ni–Ge distances in the building block **C′** range between *d*(Ge8–Ni10) = 2.333(4) Å

and d(Ge7–Ni5) = 2.499(3) Å, which are similar to those in the building block **B′** in $Ca_{15}Ni_{68}Ge_{37}$, while the Ni–Ni distances range from d(Ni1–Ni1) = 2.598(5) Å to d(Ni2–Ni5) = 2.833(2) Å.

In analogy to the description of $CaNi_5Ge_3$, the projection of $Ca_{15}Ni_{68}Ge_{37}$ along the c axis shows two layers, α and β (Figure 5). The layer α consists of "$Ni_{42}Ge_{22}$" per unit cell, while the layer β has a unit cell composition of "$Ca_{15}Ni_{24}Ge_{15}$". The Ca atoms are situated only in the layer β as observed for $CaNi_5Ge_3$. In $Ca_{15}Ni_{68}Ge_{37}$, one-dimensional $^1_\infty[Ni_3Ge]$ ribbons are found that have the Ni_3Ge structure. The Ca-centered hexagonal Ni-Ge prisms, which have been described above, are a result of their arrangement at a 60° angle. No Ge–Ge contacts occur as the $^1_\infty[Ni_3Ge]$ ribbons, with their neighbouring Ge atoms, are not arranged in a parallel way (as in the two-dimensional layers in $CaNi_5Ge_3$).

The crystal structure of $Ca_{15}Ni_{68}Ge_{37}$ can be compared to that of $Sr_2Au_3In_4$.[14] Here a trigonal rod of three distorted hexagonal prisms, which are each centered by a Sr atom, is surrounded by a three-dimensional network of hexagonal and pentagonal prisms, just as the building block **C′** is enclosed by the network **B′**. The three-dimensional network and the trigonal units in $Sr_2Au_3In_4$ are connected via a structural element of the polyanionic network in $ThCr_2Si_2$,[35] just as the **C′** and **B′** units in $Ca_{15}Ni_{68}Ge_{37}$ are interconnected by means of the Ni_3Ge (**A′**) structural element.

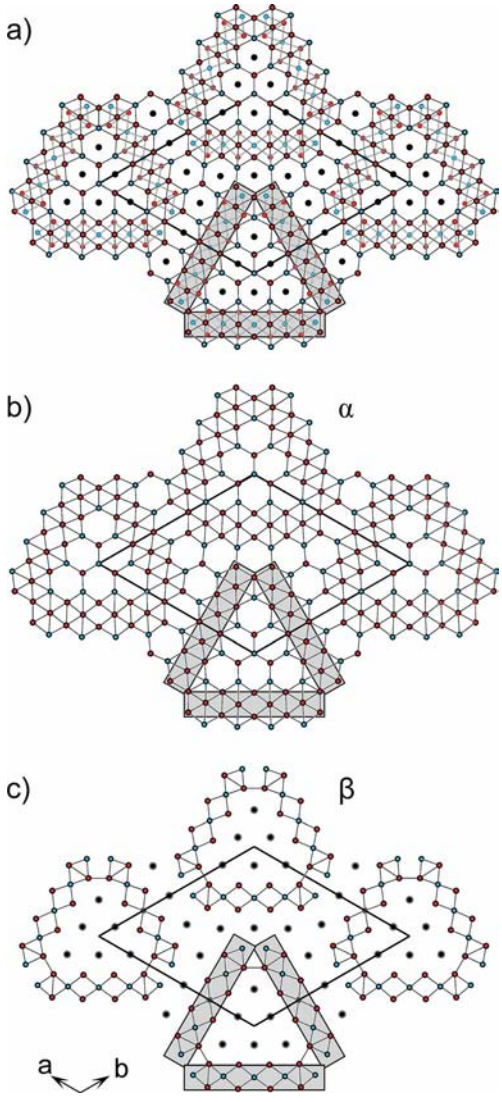

Figure 5. (a) The crystal structure of $Ca_{15}Ni_{68}Ge_{37}$ as a projection along the c axis. The two layers, (b) α at z = 0 and (c) β at z = ½, are given. The sections that are deduced from the Ni_3Ge structure type are highlighted in grey. The Ca atoms are drawn as black spheres and the Ge and Ni atoms are drawn as blue and red ones, respectively.

Crystal Structure of $Ca_7Ni_{48.9(4)}Ge_{22.1(4)}$

The compound $Ca_7Ni_{48.9(4)}Ge_{22.1(4)}$ crystallizes in its own structure type with space group *P6/mmm* [Z = 1, a = 17.381(4) Å, c = 4.046(1) Å]. As for $Ca_{15}Ni_{68}Ge_{37}$, the crystal structure may be derived from the structural motifs found in $CaNi_5Ge_3$. As shown in Figure 6, there are three structural motifs that dominate the structure. The structural unit **A″** (Figure 6, b) can be deduced from the Ni_3Ge structure, the coordination polyhedra of Ca2 (Figure 6, c) are labelled as **B″**, and the coordination polyhedra of Ca1 (Figure 6, d) are labelled as **C″**.

The structural motif **A″**, which connects the units **B″** and **C″**, is shown in Figure 6 (c). As described above, in the most Ca rich phase, $Ca_{15}Ni_{68}Ge_{37}$, the segments of the Ni_3Ge structure form one-dimensional trigonal units. In $CaNi_5Ge_3$, which has a medium Ca content, the segments of the Ni_3Ge structure form two-dimensional layers. In contrast, in $Ca_7Ni_{48.9(4)}Ge_{22.1(4)}$, which has the lowest Ca content, ribbons of the Ni_3Ge structure are more connected and form a trigonal framework in the *ab* plane that results in an overall three-dimensional Ni-Ge substructure. The $^1_\infty[Ni_{3+x}Ge_{1-x}]$ ribbons that are found in $Ca_7Ni_{48.9(4)}Ge_{22.1(4)}$ (building block **A″**) are more narrow than those found in $Ca_{15}Ni_{68}Ge_{37}$; they are three edge sharing Ni centered distorted cubes wide. The ribbons are once again arranged at a 60° angle. Singular columns of condensed Ca centered hexagonal face sharing Ni-Ge prisms (building block **B″**) and rods of three parallel condensed piles, which retain the trigonal structure of the Ni-Ge network (building block **C″**), are observed in the resulting framework.

The $^1_\infty[Ni_{3+x}Ge_{1-x}]$ ribbons of $Ca_7Ni_{48.9(4)}Ge_{22.1(4)}$ (**A″**) consist of two ribbons of distorted square layers of Ni atoms (Ni2, Ni3, Ni4, Ni5), which result from the rectangular outer faces of the unit **C″**, with a further ribbon of a square layer of alternating Ni and Ge atoms (Ni6, Ni7, Ge4, Ge1/Ni1) between the two ribbons. The resulting Ni6 and Ni7 coordination polyhedra are distorted cubes of Ni atoms that are capped by six Ge atoms. The resulting Ge4 coordination polyhedron is a distorted cuboctahedron of Ni atoms. The structural motif **A″** corresponds to a low-dimensional section of Ni_3Ge, as it is similarly found in

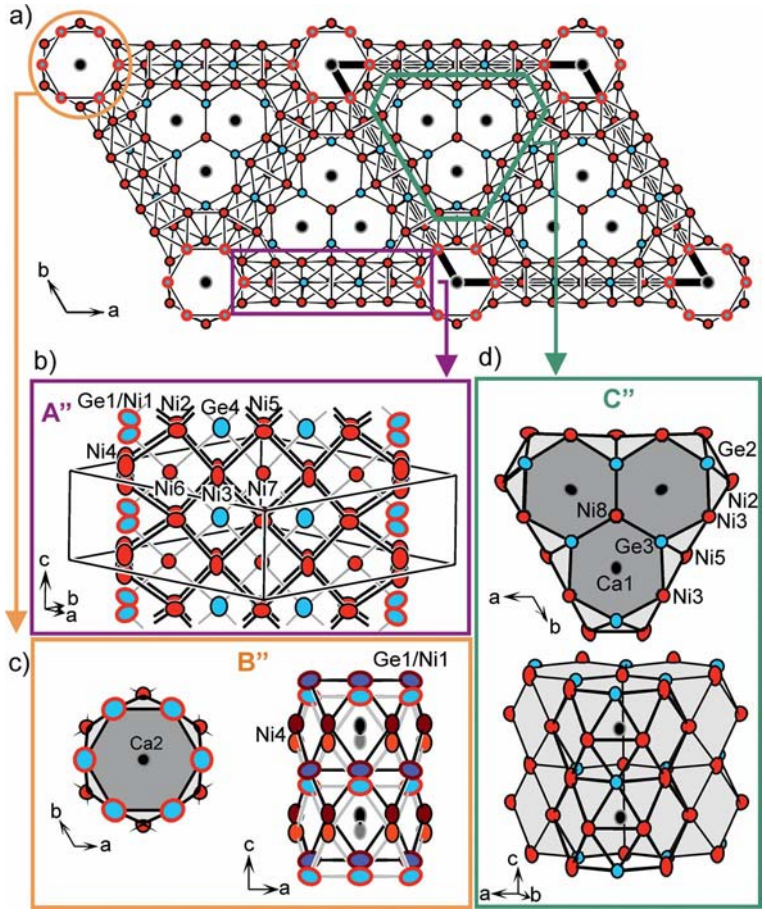

Figure 6. (a) The crystal structure of $Ca_7Ni_{48.9(4)}Ge_{22.1(4)}$ indicating different structure motifs: (b) the Ni_3Ge type segment that is built from the coordination polyhedra of Ni6, Ni7, and Ge4 (labelled **A**′′), (c) the coordination polyhedra of Ca2 (labelled **B**′′), and (d) the building block that results from the coordination polyhedra of Ca1 (labelled **C**′′). The Ca atoms are drawn as black spheres and the Ge and Ni atoms are drawn as blue and red ones, respectively. The mixed position of Ni1/Ge1 is drawn as a blue sphere with red borderlines. The chosen Ni–Ge bonds are given for a better understanding of the structure and emphasize the different structural motifs. The displacement ellipsoids in (b) to (d) are drawn at the 95% probability level.

$CaNi_5Ge_3$ (**A**) and in $Ca_{15}Ni_{68}Ge_{37}$ (**A**′). Consequently, a similar compression of the cuboids and, thus, a similar variation in the bond length is observed. In $Ca_7Ni_{48.9(4)}Ge_{22.1(4)}$, the distances between the vertices of the distorted cubes and the centering Ge and Ni atoms [from *d*(Ge4–Ni2) = 2.389(2) Å to *d*(Ni3–Ni6) = 2.545(2) Å] are significantly shorter than the distance between the centering Ge atoms and the centering Ni atoms [*d*(Ge4–Ni7) = 2.782(1) Å and *d*(Ge4–Ni6) = 3.054(2) Å] as well as the distances between the Ni atoms within the distorted square Ni layers [from *d*(Ni2–Ni3) = 2.737(1) Å to *d*(Ni3–Ni5) = 2.885(1) Å]. The interlayer distances between the distorted square Ni layers are comparable to those observed in $CaNi_5Ge_3$ and $Ca_{15}Ni_{68}Ge_{37}$ [from *d*(Ni2–Ni2) = 2.647(2) Å to *d*(Ni5–Ni5) = 2.910(3) Å].

In Figure 7, the structure is represented in terms of the layers seen along the *c* axis. Two layers, α and β, alternate along the *c* axis in $Ca_7Ni_{48.9(4)}Ge_{22.1(4)}$. The α layer consists of "$CaNi_{29}Ge_{12}$" while the β layer has a composition of "$Ca_6Ni_{20}Ge_{10}$" per unit cell. In contrast to the other two title compounds, both the α and β layers contain Ca atoms, which seems to have a crucial impact on the structure.

Parts (b) and (c) of Figure 7 illustrate that six $^1_\infty[Ni_{3+x}Ge_{1-x}]$ ribbons join to form one hexagonal prism. The outermost atoms of these ribbons (Ni4 and Ni1/Ge1) construct the coordination polyhedron of Ca2 (**B**′′, Figure 6, c). The hexagonal prism is formed by a mixed site of approximately 1/3 Ni1 and 2/3 Ge1. The rectangular sides are capped by Ni4 atoms. This rod of capped hexagonal prisms $Ca@Ge_8Ni_{10}$ can be described by the Niggli formula $^1_\infty[Ca(Ni_{6(1-x)}Ge_{6x})_{2/2}Ni_{6/1}]$ with $x = 0.68(6)$ (*x*: occupancy of Ge1 on the Ge1/Ni1 position). It is interesting to note that the resulting Ni/Ge ratio of about 1:2 corresponds to the Ni/Ge ratio observed in the hexagonal prisms of $CaNi_5Ge_3$, in which no disorder is present. The merging of six $^1_\infty[Ni_{3+x}Ge_{1-x}]$ (with $x = 0$) ribbons around the Ca2 atom (Figure 7) would result in a Ge_6 hexagon in contrast to the Ni_3Ge_3 and Ni_4Ge_2 hexagons observed in $Ca_{15}Ni_{68}Ge_{37}$ or $Ca_7Ni_{48.9(4)}Ge_{22.1(4)}$ and $CaNi_5Ge_3$, respectively. Thus, a structural frustration, which leads to a mixed occupancy of Ni1 and Ge1, occurs.

Furthermore, a disorder of all of the positions of the building block **B**′′ (Ca2, Ge1/Ni1, and Ni4) is observed. The sites under consideration are split around the crystallo-

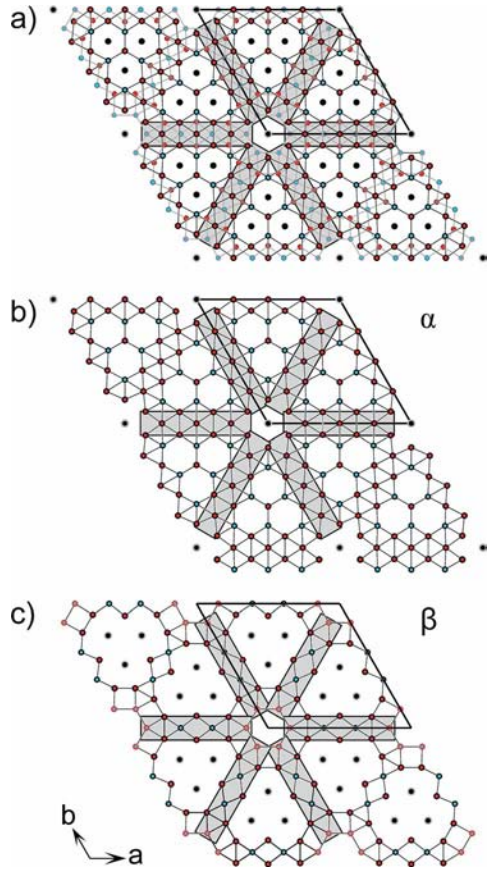

Figure 7. (a) The crystal structure of $Ca_7Ni_{48.9(4)}Ge_{22.1(4)}$. The two layers, (b) α at $z = 0$ and (c) β at $z = ½$, are given. The sections that are deduced from the Ni_3Ge structure type are highlighted in grey. The Ca atoms are drawn as black spheres and the Ge and Ni atoms are drawn as blue and red ones, respectively. The mixed position, Ge1/Ni1, is given as a blue sphere with red borderlines.

graphic mirror plane that is perpendicular to the *c* axis. The short interatomic distances that result between the split positions are not discussed, but each set of split positions leads to a realistic structure. The distance between Ni1/Ge1 and Ni4 [2.449(2) Å] of such a set of split positions is comparable to those found in *fcc* Ni [*d*(Ni–Ni) = 2.49 Å[36]] and to the Ni–Ge distances found in other polar intermetallics in the Ca/Ni/Ge system. The Ni1/Ge1–Ni1/Ge1 distance [2.635(2) Å] in $Ca_7Ni_{48.9(4)}Ge_{22.1(4)}$ is longer than the Ni–Ge distances that are observed in the $CaNi_5Ge_3$ and $Ca_{15}Ni_{68}Ge_{37}$ hexagons. In $CaNi_5Ge_3$ and $Ca_{15}Ni_{68}Ge_{37}$ the distances between the capping Ni atoms and the centering Ca atoms are between 3.0 and 3.3 Å. In contrast, the corresponding distance for one set of split positions in the building block **B**′′ of $Ca_7Ni_{48.9(4)}Ge_{22.1(4)}$ is significantly shorter [*d*(Ca2–Ni4) = 2.885(2) Å]. These shorter distances may have led to a displacement of the Ca2 out of the plane of the Ni4 atoms, which consequently resulted in longer distances [*d*(Ca2–Ni4) = 2.982(3) Å] and further split positions in the hexagonal prism.

The coordination polyhedron of Ca1 (**C**′′, Figure 6, d) represents a hexagonal prism, which is built from two distorted planar Ni_3Ge_3 hexagons that have alternating Ge (Ge2 and Ge3) and Ni (Ni3 and Ni8) atoms at the vertices. Three of these hexagonal prisms are condensed by means of two rectangular sides each. The Ni8 atom is shared by all three of the hexagons and the Ge3 atoms are shared by two of the hexagons. This building block alternatively can be described as a condensation of three rods that have the formulae $^1_\infty[Ca(Ni_{3/1}Ge_{3/1})_{2/2}]$ to $^1_\infty[\{Ca(Ni_{2/1}Ge_{1/1}Ge_{2/2}Ni_{1/3})_{2/2}\}_3]$. The resulting outer rectangular faces are capped by Ni atoms: the Ni2 atoms cap the rectangular sides that are made up of Ni3 and Ge2, while the Ni5 atoms cap the rectangular sides that are made up of the Ni3 and Ge3 atoms of the two coordination polyhedra at once. From the above description, the whole structure motif **C**′′ can be rationalized as $^1_\infty[\{Ca(Ni_{2/1}Ge_{1/1}Ge_{2/2}Ni_{1/3})_{2/2}Ni_{2/1}Ni_{2/2}\}_3]$ or, in a molecular approach, as $Ca_3@Ge_{12}Ni_{23}$. The Ni–Ge distances in this building block range from 2.337(2) Å to 2.435(2) Å and are comparable to the Ni–Ge distances in other intermetallic compounds. In contrast, the Ni–Ni distances [from 2.500(2) Å to 2.885(1) Å] are longer than the distance found in *fcc* Ni.

The **C**′ building block of $Ca_{15}Ni_{68}Ge_{37}$ and the **C**′′ building block of $Ca_7Ni_{48.9(4)}Ge_{22.1(4)}$ are closely related to the main structural motifs of the compounds of the $R_{n(n-1)}T_{(n+1)(n+2)}X_{n(n+1)+1}$ series ($n = 3$ and $n = 4$; R = Zr or rare earth, T = 3d or 4d transition metal, X = P) that were mentioned in the introduction. A further closely related structural motif has been described for $Sr_2Au_3In_4$[14] and for $Sr_4Au_9In_3$.[15] Here, the triangular units of the three Sr-centered hexagonal prisms of Au and In are capped by the In atoms. In the *Ae*/Ni/Ge system (*Ae* = Ca, Sr, Ba), the compounds $SrNi_2Ge$ and $SrNi_3Ge_2$[37] need to be mentioned since they have a similar cation coordination. Condensed welded hexagonal prisms, which are centered by the Sr atoms and have alternating Ni and Ge atoms at the vertices, are found in both of the compounds. In both cases, the Ni and Ge atoms form two-dimensional layers.

Magnetic Properties of $CaNi_5Ge_3$

The plot of the molar magnetic susceptibility, χ_m, of $CaNi_5Ge_3$ as a function of temperature in the range of 1.8 to 300 K is presented in Figure S1 (see Supporting Information). The raw magnetization data were corrected for the holder contribution and were converted to molar susceptibility (χ_m). The magnetic susceptibilities were corrected for the diamagnetic contribution of the core electrons. The compound exhibits temperature-independent Pauli paramagnetic behavior over 10 to 300 K where the susceptibility varies between approximately 5×10^{-4} to 6×10^{-4} emu/mol. The increase in the molar susceptibility below 10 K probably arises from the presence of a small amount of ferromagnetic impurities (most probably Ni). No indication of superconductivity is observed in the measured temperature interval.

Electronic Structure of $CaNi_5Ge_3$ Emphasizing Ge–Ge Bonds

The homoatomic Ge–Ge bonds with a distance of 2.551(3) Å are a result of the primitive stacking of the layers of the Ni_3Ge structure and its neighbouring Ge atoms (Ge2 and Ge3) along the *c* direction in $CaNi_5Ge_3$. These bonds are not observed in the other title compounds since in $Ca_{15}Ni_{68}Ge_{37}$ and $Ca_7Ni_{48.9(4)}Ge_{22.1(4)}$ the one-dimensional Ni_3Ge ribbons are arranged at a 60° angle. Nevertheless for $Ca_7Ni_{48.9(4)}Ge_{22.1(4)}$, a ratio of 1:2 (Ni/Ge) is observed for the Ni1/Ge1 position, but, due to the structural disorder, the Ge–Ge bonds are not unambiguously established.

In order to gain a better understanding of the chemical bonding situation in $CaNi_5Ge_3$, especially concerning the homoatomic Ge–Ge bonds, we performed electronic structure calculations. The total and the partial density of states (DOS) (given in the Supporting Information, Figure S2) reveal the metallic property of $CaNi_5Ge_3$. The DOS can be divided into two sections: the Ge (s) orbitals are associated with the energy range between –12 and –8 eV, while the states above –7 eV belong mainly to the Ge (p), Ni (d), and Ca (d) orbitals. The different coordinations of the Ge atoms are reflected in the Ge (s) states: the peaks that correspond to the Ge1 (s) state, which is coordinated to 12 Ni atoms, are broad and flat. In contrast, the Ge2 and Ge3 (s) states, which are coordinated to 5 Ni and 1 Ge atoms, have sharp peaks. Similarly, the different coordinations are reflected in the peaks associated with the Ni (d) and the Ge (p) states.

Furthermore, the integrated crystal orbital Hamilton populations (–iCOHPs) (Table 3) and the contour line diagrams of the electron localization function (ELF) (Figure 8)

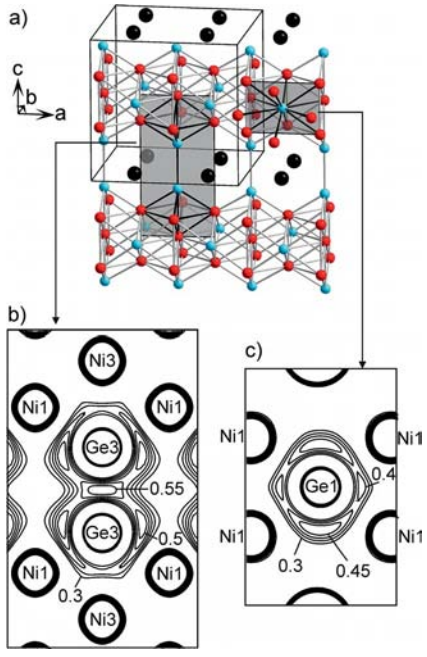

Figure 8. (a) The structure of $CaNi_5Ge_3$ indicating the two-dimensional sections shown in Figure (b) and (c): (b) the contour line diagram of the ELF in steps of 0.05, which includes the Ge3–Ge3 bond, and (c) the contour line diagram of the ELF in steps of 0.05, which is parallel to the *ac* plane through the Ge1 atom.

were calculated. In Figure 8, two contour line diagrams of the ELF are presented and show the *ac* planes through the Ge1 and Ge3 atoms. The contour line diagram that corresponds to the *ac* plane through Ge2 is analogous to the one through Ge3. In accordance with the high –iCOHP values for the Ge–Ge bonds [–iCOHP (Ge2–Ge2) = 1.84 eV and –iCOHP (Ge3–Ge3) = 2.03 eV], a bisynaptic valence basin of the ELF is observed below η = 0.6. At slightly lower values, namely, below η = 0.55, four monosynaptic basins that are associated with Ge2/Ge3 are observed (Figure 8, b). This is in good agreement with the ELF calculated for the Ge–Ge bond in $CaNi_2Ge_2$,[24] which has very similar characteristics. At values below η = 0.49, two monosynaptic basins at opposite sites of Ge1 are observed (Figure 8, c), which merge at lower ELF values. The –iCOHP values approximately mirror the bond lengths. However, the Ge–Ge bonds generally have higher values than the Ni–Ge bonds, even though the bond lengths are similar. Furthermore, high –iCOHP values were calculated for the Ni–Ge contacts, but no bisynaptic valence basins of the ELF between the Ni and Ge atoms are observed.

Conclusion

The title compounds, which all have a complex network of Ni and Ge atoms, provide a new class of compounds in the *Ae*/Ni/Ge system (*Ae*: Ca, Sr, Ba). The intermetallic phases that have been previously described in these systems contain two-dimensional [Ni_xGe_y] layers (such as CaNiGe, $Ca_2Ni_3Ge_2$, $SrNi_2Ge$, $SrNi_3Ge_2$,[37] and $BaNi_2Ge_2$[38]) as well as simple three-dimensional networks ($CaNi_2Ge_2$, $CaNiGe_3$, $CaNiGe_2$, $SrNi_2Ge_2$,[25] and $SrNiGe_2$[26]). This wide variety of structures is now extended to complex three-dimensional structures and underlines the complex interactions between the components in the *Ae*/Ni/Ge system. The similar compositions of the title compounds result in the presence of common structural motifs. Further is the comparison between the title compounds and the intermetallic phases found in the U/*T*/Si (*T*: Co, Fe) system most remarkable. $CaNi_5Ge_3$ crystallizes in a structure type that is very similar to that of UFe_5Si_3, while $Ca_7Ni_{48.9(4)}Ge_{22.1(4)}$ and $Ca_{15}Ni_{68}Ge_{37}$ can be compared to the compounds in the $R_{n(n+1)}T_{6(n^2+1)}Si_{2(2n^2+1)}$ series, which has $U_6Co_{30}Si_{18}$ (UCo_5Si_3), $U_{12}Co_{60}Si_{38}$, and $U_{20}Co_{102}Si_{66}$ as its representatives. This indicates the similarities between the interactions that determine the crystal structure in both systems. Further research in this field is necessary in order to gain a better understanding of the parameters that influence the structure.

By regarding the title compounds as polar intermetallics the following conclusions can be drawn: the Ni-Ge framework of the intermetallic Ni_3Ge compound is broken apart by the Ca atoms, which is just like the elemental structures in the Zintl phases. An increasing Ca content leads to the formation of low-dimensional structures that retains the structure features of Ni_3Ge. In the series studied in this paper, namely, $Ca_7Ni_{48.9(4)}Ge_{22.1(4)}$, $CaNi_5Ge_3$, and

$Ca_{15}Ni_{68}Ge_{37}$, an increasing Ca content leads to three-, two-, and one-dimensional Ni-Ge substructures, respectively. This is comparable to the series of the Zintl phases, $CaSi_2$,[39] CaSi,[40] and Ca_2Si,[41] in which the Ca scissors the Si diamond structure with the formation of two-, one-, and zero-dimensional Si substructures.

Experimental Section

Syntheses: All manipulations were performed in an argon-filled glove box (H_2O and O_2 levels < 0.1 ppm). The starting materials for the synthesis of $CaNi_5Ge_3$, $Ca_{15}Ni_{68}Ge_{37}$, and $Ca_7Ni_{48.9(4)}Ge_{22.1(4)}$ were ingots of calcium (Alfa Aesar, purity 99.5%), nickel wire (Ø = 1 mm, Johnson–Matthey, purity 99.98%), and germanium pieces (ChemPur, purity 99.999%). The amounts of the elements, which corresponded to a total mass of 0.7 g, were varied. The samples that were used for the single-crystal X-ray diffraction analysis were obtained by using the following ratios of Ca/Ni/Ge: 1:5:3 for $CaNi_5Ge_3$, and 8:53:18 for $Ca_{15}Ni_{68}Ge_{37}$ and $Ca_7Ni_{48.9(4)}Ge_{22.1(4)}$ (different samples). The fact that the two latter compounds were obtained by using the same sample loading indicates that the synthesis is very sensitive to variations during the arc melting and the subsequent heat treatment. The pieces of nickel and germanium were arc-melted (Mini Arc Melting System, MAM-1, Johanna Otto GmbH) and then calcium was added. For both of the steps, the resulting reguli were arc-melted and turned over three times in order to ensure homogeneity. After these melting procedures, only samples of low crystallinity were obtained. In order to grow single crystals for $Ca_{15}Ni_{68}Ge_{37}$ and $Ca_7Ni_{48.9(4)}Ge_{22.1(4)}$, the reguli obtained after the arc-melting were sealed in tantalum ampoules (Mini Arc Melting System, MAM-1, Johanna Otto GmbH) and placed in a water-cooled sample chamber of an induction furnace (Hüttinger Elektronik, Freiburg, Typ TIG 2.5/300). In the induction furnace the ampoules that contained the samples of $Ca_{15}Ni_{68}Ge_{37}$ and $Ca_7Ni_{48.9(4)}Ge_{22.1(4)}$ were heated under flowing argon up to approximately 1140 °C and 1220 °C for five minutes and then held at 1060 and 1150 °C for 60 min, respectively. After the melting procedure, the samples were cooled over half an hour to approximately 850 °C and then cooled down to room temperature in about one minute by switching off the furnace. A special heat treatment was needed for the growth of suitable single crystals for the structure determination of $CaNi_5Ge_3$. The arc-melted regulus of $CaNi_5Ge_3$ was crushed, powdered, and cold-pressed to pellets. It was then placed into a tantalum container and enclosed in an evacuated silica tube, which was placed in a muffle furnace (LOBA, HTM Reetz GmbH). The sample was heated to 950 °C and held at this temperature for 12 h. The temperature was then lowered at a rate of 6 °C/h to 650 °C, held at this temperature for 120 h, and finally cooled to room temperature over 3 hours. The light grey samples were easily separated from the tantalum crucibles by deforming the crucibles. No reaction between the samples and the crucible material was detected by visual control or by powder X-ray diffraction. All three of the samples were grey and were stable in air and moisture. Needle-like (for $Ca_{15}Ni_{68}Ge_{37}$ and $Ca_7Ni_{48.9(4)}Ge_{22.1(4)}$) and plate-like (for $CaNi_5Ge_3$) single crystals with a metallic lustre were isolated.

Single-Crystal and Powder X-ray Diffraction Studies and Structure Refinement: The purity of the samples was checked with a STOE STADI P powder X-ray diffractometer by using Cu-$K_{\alpha1}$ radiation. The powder X-ray diffraction diagrams of the samples, in which the single crystals that will be discussed later were found, showed that the sample of $CaNi_5Ge_3$ was pure, the sample of $Ca_{15}Ni_{68}Ge_{37}$ contained an unknown phase and small amounts of $Ca_{10}Ni_{34}Ge_{16}$,[42] whereas the sample of $Ca_7Ni_{48.9(4)}Ge_{22.1(4)}$ contained $Ca_{15}Ni_{68}Ge_{37}$, $Ca_{10}Ni_{34}Ge_{16}$, and small amounts of an unknown phase as the impurities. The lattice parameters (see Table 1) of $Ca_{15}Ni_{68}Ge_{37}$ and $Ca_7Ni_{48.9(4)}Ge_{22.1(4)}$ were obtained from the least-squares fit of these powder X-ray diffraction data with WinXPOW.[43] For $CaNi_5Ge_3$, a Rietveld refinement was performed by using the Fullprof Suite.[44] The measured powder X-ray diffraction diagrams are given in the Supporting Information (Figures S3, S4, and S5). In all of the cases, the lattice parameters that were determined from the powder X-ray diffraction patterns and from the single-crystal X-ray diffraction data agreed well.

The single crystals of the title compounds were fixed on the top of a glass fibre in air by using nail polish. The single-crystal X-ray diffraction intensity data were collected at room temperature with an Oxford Diffraction Xcalibur3 diffractometer for $CaNi_5Ge_3$ and $Ca_7Ni_{48.9(4)}Ge_{22.1(4)}$ and an IPDS 2T diffractometer for

Table 1. The crystallographic data for $CaNi_5Ge_3$, $Ca_{15}Ni_{68}Ge_{37}$, and $Ca_7Ni_{48.9(4)}Ge_{22.1(4)}$.

Empirical formula	$CaNi_5Ge_3$	$Ca_{15}Ni_{68}Ge_{37}$	$Ca_7Ni_{48.9(4)}Ge_{22.1(4)}$
Formula weight [g/mol]	551.40	7279.31	4754.33
Space group, Z	*P*4/*mbm* (127), 4	$P\bar{6}2m$ (189), 1	*P*6/*mmm* (191), 1
a [Å]	8.0855(1)	22.436(2)	17.381(4)
c [Å]	7.8466(1)	3.9684(4)	4.046(1)
V [Å^3]	512.97(1)	1729.9(3)	1058.5(4)
Calculated density [g/cm^3]	7.140	6.987	7.458
Absorption coefficient [mm^{-1}]	36.09	34.87	37.35
F(000)	1024	3388	2216
Crystal size [mm^3]	0.02× 0.08× 0.09	0.04× 0.04× 0.08	0.04× 0.05× 0.09
θ range [°]	3.6 to 30.0	3.6 to 29.2	3.6 to 30.5
Index ranges (h,k,l)	(–10/11), ±11, ±11	(–29/30), ±30, ±5	(–24/18), (22/24), ±5
Reflections collected	10980	33224	19123
Independent reflections (R_{int})	439 (0.045)	1849 (0.156)	693 (0.048)
Reflections with $I \geq 2\sigma(I)$ (R_σ)	302 (0.013)	1758 (0.048)	550 (0.015)
Data/parameters	439/31	1849/133	693/59
GOF on F^2	1.096	1.522	1.108
R_1/wR_2 [$I > 2\sigma(I)$]	0.023/0.049	0.049/0.095	0.027/0.080
R_1/ wR_2 (all data)	0.043/0.054	0.053/0.096	0.035/0.082
Extinction coefficient	0.0014(2)	–	0.0011(2)
Largest diff. peak/hole [e/Å^3]	0.71/ –0.67	2.25/–3.01	1.55/–1.50

$Ca_{15}Ni_{68}Ge_{37}$. Both diffractometers used graphite monochromatized Mo-K_α (0.71073 Å) radiation. The raw data were corrected for background, polarization, and Lorentz factor. Empirical absorption correction was applied to the data for $Ca_7Ni_{48.9(4)}Ge_{22.1(4)}$,[45] whereas the data were numerically corrected for $CaNi_5Ge_3$ and $Ca_{15}Ni_{68}Ge_{37}$.[46,47] The structures were solved by direct methods (SHELXS-97)[48] and were subsequently refined (full-matrix least-squares on F_o^2) with anisotropic atomic displacement parameters for all of the atoms (SHELXL-97).[49] The coordinates of the atomic positions were chosen as suggested by the program STRUCTURE TIDY.[50] In the case of $Ca_{15}Ni_{68}Ge_{37}$, the measured crystal was an inversion twin with equal volume domains. In $Ca_7Ni_{48.9(4)}Ge_{22.1(4)}$; a mixed occupancy for Ni1/Ge1 occurred on the 2*d* site. The mirror plane that is perpendicular to the *c* axis causes a superposition of the two rods of the hexagonal prisms $^1{}_\infty[Ca(Ni_{6(1-x)}Ge_{6x})_{2/2}Ni_{6/1}]$ with $x = 0.68(6)$, constructed from the atoms Ni1/Ge1 and Ni4 (see results and discussion). The removal of this mirror plane in the space group symmetry combined with twin refinements could not resolve this disorder. However, there were some hints in the diffraction pattern that pointed towards a partially ordered structure. A thorough inspection of the *hkn* layers showed diffuse maxima that were centered at positions n***a**$^*_{sub}$/3 and n***b**$^*_{sub}$/3. Due to its very low intensities and the diffusity of the reflections, a refinement of the superstructure failed.

Table 2. The atomic coordinates and the isotropic equivalent displacement parameters for $CaNi_5Ge_3$, space group *P*4/*mbm*; $Ca_{15}Ni_{68}Ge_{37}$, space group $P\bar{6}2m$; and $Ca_7Ni_{48.9(4)}Ge_{22.1(4)}$, space group *P*6/*mmm*.

Atom	Occ. ≠ 0	Wyckoff position	*x*	*y*	*z*	U_{eq}
$CaNi_5Ge_3$						
Ca		4 *g*	0.2490(2)	0.7490(1)	0	11(1)
Ge1		4*h*	0.2368(1)	0.7368(1)	1/2	14(1)
Ge2		4*f*	0	1/2	0.8340(2)	10(1)
Ge3		4*e*	0	0	0.8374(2)	8(1)
Ni1		16*l*	0.0147(1)	0.2486(2)	0.6798(1)	3(1)
i2		2*c*	0	1/2	1/2	10(1)
Ni3		2*b*	0	0	1/2	10(1)
$Ca_{15}Ni_{68}Ge_{37}$						
Ca1		6*k*	0.2176(2)	0.5663(2)	1/2	14(1)
Ca2		3 *g*	0.2036(2)	0.2036(2)	1/2	14(1)
Ca3		3 *g*	0.4541(2)	0	1/2	13(1)
Ca4		3 *g*	0.1051(2)	0	1/2	15(1)
Ge1		6*k*	0.3934(1)	0.4703(1)	1/2	13(1)
Ge2		6*k*	0.1981(1)	0.3801(1)	1/2	15(1)
Ge3		6*j*	0.1016(1)	0.2079(1)	0	12(1)
Ge4		6*j*	0.3208(1)	0.5567(1)	0	11(1)
Ge5		6*j*	0.1090(1)	0.4645(1)	0	11(1)
Ge6		3 *g*	0.2866(2)	0	1/2	10(1)
Ge7		3*f*	0.3106(2)	0.3106(2)	0	14(1)
Ge8		1*a*	0	0	0	16(1)
Ni1		6*k*	0.2907(2)	0.3575(2)	1/2	14(1)
Ni2		6*k*	0.0984(2)	0.2654(2)	1/2	15(1)
Ni3		6*k*	0.3004(2)	0.4920(2)	1/2	15(1)
Ni4		6*k*	0.1042(2)	0.4034(2)	1/2	16(1)
Ni5		6*j*	0.2025(2)	0.3169(2)	0	14(1)
Ni6		6*j*	0.4241(2)	0.5405(2)	0	15(1)
Ni7		6*j*	0.3126(2)	0.4310(1)	0	13(1)
Ni8		6*j*	0.1014(2)	0.3353(2)	0	14(1)
Ni9		6*j*	0.2093(2)	0.4492(2)	0	14(1)
Ni10		3*f*	0.1040(2)	0.1040(2)	0	14(1)
Ni11		3*f*	0.4236(2)	0.4236(2)	0	18(1)
Ni12		3*f*	0.3527(2)	0	0	16(1)
Ni13		3*f*	0.2189(2)	0	0	15(1)
Ni14		2*c*	2/3	1/3	0	15(1)
$Ca_7Ni_{48.9(4)}Ge_{22.1(4)}$						
Ca1		6*m*	0.2552(1)	0.5104(2)	1/2	11(1)
Ca2	0.50	2*e*	0	0	0.085(2)	14(2)
Ge1/Ni1	0.34(3)/0.16(3)	12*n*	0.1516(2)	0.1516(2)	0.4090(4)	25(1)
Ge2		6*l*	0.1762(1)	0.3523(1)	0	11(1)
Ge3		6*l*	0.5890(1)	0.1781(1)	0	10(1)
Ge4		6*k*	0.3901(1)	0	1/2	17(1)
Ni2		12*q*	0.0880(1)	0.3197(1)	1/2	15(1)
Ni3		12*p*	0.0914(1)	0.4274(1)	0	15(1)
Ni4	0.50	12*o*	0.0958(1)	0.1916(1)	0.1030(5)	20(1)
Ni5		6*m*	0.5483(1)	0.0967(1)	1/2	14(1)
Ni6		6*j*	0.2585(1)	0	0	11(1)
Ni7		3*f*	½	0	0	10(1)
Ni8		2*c*	1/3	2/3	0	12(1)

Table 3. The interatomic distances [Å] calculated with the lattice parameters, that are taken from the powder X-ray diffraction data, and the corresponding integrated crystal orbital Hamilton population (iCOHPs) values at E_F for $CaNi_5Ge_3$. All of the –iCOHP values are in eV per bond per cell. The interatomic distances of $Ca_{15}Ni_{68}Ge_{37}$ and $Ca_7Ni_{48.9(4)}Ge_{22.1(4)}$ are given in the Supporting Information (Table S1).

		Distance [Å]	–iCOHP [eV]			Distance [Å]	–iCOHP [eV]
Ge1	Ni1	2.4578(7) (4×)	1.69	Ge3	Ni1	2.363(2) (4×)	2.21
	Ni1	2.4773(7) (4×)	1.64		Ge3	2.551(3) (1×)	2.03
	Ni2	2.7071(9) (1×)	1.02		Ni3	2.648(2) (1×)	1.01
	Ni3	2.8627(6) (2×)	0.73		Ca1	3.1303(6) (4×)	
	Ni2	3.0102(9) (1×)	0.51				
				Ni1	Ni3	2.4587(9) (1×)	1.07
Ge2	Ni1	2.369(2) (4×)	2.37		Ni2	2.4774(9) (1×)	
	Ge2	2.605(4) (1×)	1.84		Ni1	2.707(2) (1×)	0.74
	Ni2	2.621(2) (1×)	1.06		Ni1	2.822(2) (1×)	0.45
	Ca1	3.131(2) (2×)			Ni1	2.847(2) (2×)	0.52
	Ca1	3.152(2) (2×)			Ni1	3.042(2) (1×)	0.27
					Ca1	3.1565(7) (1×)	
					Ca1	3.2946(7) (1×)	

All of the relevant data of the structure determination and evaluation are listed in Table 1.

The positional parameters and selected interatomic distances are given in Tables 2, 3, and S1 (see Supporting Information). Further details on the crystal structure investigation(s) may be obtained from the Fachinformationszentrum Karlsruhe, 76344 Eggenstein-Leopoldshafen, Germany (fax: +49-7247-808-666; e-mail: crysdata@fiz-karlsruhe.de) on quoting the depository numbers CSD-422815 (for $CaNi_5Ge_3$), -422814 (for $Ca_{15}Ni_{68}Ge_{37}$), and -422813 (for $Ca_7Ni_{48.9(4)}Ge_{22.1(4)}$).

The composition of the crystals that were used for the single-crystal X-ray determination were checked with a JEOL SEM 5900LV scanning electron microscope. A qualitative EDX analysis of the well-shaped single crystals revealed the presence of all three of the elements, namely, Ca, Ni, and Ge, and the absence of elements heavier than Na.

Magnetic Susceptibility Measurements: The DC magnetization data were collected with a Quantum Design MPMS XL5 superconducting quantum interference device (SQUID). The temperature-dependent data were obtained by the measurement of the magnetization from 1.8 to 300 K in an applied magnetic field of 1 T by using 36 mg of $CaNi_5Ge_3$ powder that was held in a straw.

Electronic Structure Calculations: Calculations for the electronic structure of $CaNi_5Ge_3$ employed the linear muffin-tin orbital (LMTO) method in the atomic sphere approximation (ASA) by using the tight-binding (TB) program, TB-LMTO-ASA.[51] The exchange-correlation term was calculated within the local density approximation (LDA) and was parameterized according to von Barth and Hedin.[52] The radii of the muffin-tin spheres and the empty spheres were determined according to the method used by Jepsen and Andersen.[53] The basis set of the short-ranged[54] atom-centered TB-LMTOs contained s, d valence functions for Ca, s-d valence functions for Ni, and s, p valence functions for Ge. The 4p orbital for Ca, as well as the 3d orbitals for Ge, were included by using a downfolding technique.

The chemical bonding analysis was based upon theoretical partial and total density of states (DOS) curves, plots of the crystal orbital Hamilton populations (COHPs),[55] and contour line diagrams of the Electron Localization Function (ELF).[56–58] From the COHP analyses, the contribution of the covalent part of a particular interaction to the total bonding energy of the crystal can be obtained.

Supporting Information (see footnote on the first page of this article): Table S1: interatomic distances for $Ca_7Ni_{48.9(4)}Ge_{22.1(4)}$ and $Ca_{15}Ni_{68}Ge_{37}$. Figure S1: magnetic susceptibility ($\chi_m = M/H$) vs. temperature (T) for $CaNi_5Ge_3$. Figure S2: total and partial DOS for $CaNi_5Ge_3$. Figures S3 to S5: powder X-ray diffraction diagrams of the samples.

[1] S. Rundqvist, *Acta Chem. Scand.* **1962**, *16*, 1–19.
[2] E. Ganglberger, *Monatsh. Chem.* **1968**, *99*, 557–565.
[3] R. Guerin, E. H. Elghadraoui, J. Y. Pivan, J. Padiou, M. Sergent, *Mater. Res. Bull.* **1984**, *19*, 1257–1270.
[4] J. Y. Pivan, R. Guerin, *J. Less-Common Met.* **1986**, *120*, 247–254.
[5] S. I. Chikhrii, V. S. Babizhetskii, S. V. Orishchin, L. G. Akselrud, Y. B. Kuzma, *Kristallografiya* **1993**, *38*, 262–265.
[6] C. Le Senechal, V. S. Babizhetsky, S. Deputier, J. Y. Pivan, R. Guerin, *Z. Anorg. Allg. Chem.* **2001**, *627*, 1325–1333.
[7] J. Y. Pivan, R. Guerin, *J. Solid State Chem.* **1998**, *135*, 218–227.
[8] J. Y. Pivan, R. Guerin, M. Sergent, *J. Solid State Chem.* **1987**, *68*, 11–21.
[9] W. Jeitschko, L. J. Terbuchte, U. C. Rodewald, *Z. Anorg. Allg. Chem.* **2001**, *627*, 2673–2679.
[10] V. Babizhetskyy, C. Le Senechal, R. Guerin, O. Isnard, K. Hiebl, *Phys. Rev. B* **2002**, *66*, 014102.
[11] Y. P. Yarmolyuk, L. G. Akselrud, E. I. Gladyshevsky, *Kristallografiya* **1978**, *23*, 942–945.
[12] Y. P. Yarmolyuk, L. G. Akselrud, V. S. Fundamensky, E. I. Gladyshevsky, *Kristallografiya* **1980**, *25*, 169–171.
[13] L. G. Akselrud, Y. P. Yarmolyuk, E. I. Gladyshevsky, *Dopov. Akad. Nauk Ukr. RSR Ser. A* **1980**, 79–81.
[14] R. D. Hoffmann, R. Pöttgen, C. Rosenhahn, B. D. Mosel, B. Kunnen, G. Kotzyba, *J. Solid State Chem.* **1999**, *145*, 283–290.
[15] A. Palasyuk, J. C. Dai, J. D. Corbett, *Inorg. Chem.* **2008**, *47*, 3128–3134.
[16] R. D. Hoffmann, R. Pöttgen, *Z. Anorg. Allg. Chem.* **1999**, *625*, 994–1000.
[17] Y. M. Prots, W. Jeitschko, *Inorg. Chem.* **1998**, *37*, 5431–5438.
[18] A. V. Gribanov, O. L. Sologub, P. S. Salamakha, O. I. Bodak, Y. D. Seropegin, V. V. Pavlyuk, V. K. Pecharsky, *J. Alloys Compd.* **1992**, *189*, L11–L13.
[19] A. Imre, A. Hellmann, A. Mewis, *Z. Anorg. Allg. Chem.* **2006**, *632*, 1145–1149.
[20] A. V. Gribanov, O. L. Sologub, P. S. Salamakha, O. I. Bodak, Y. D. Seropegin, V. K. Pecharsky, *J. Alloys Compd.* **1992**, *179*, L7–L11.

[21] G. Venturini, B. Malaman, *J. Less-Common Met.* **1990**, *167*, 45–52.
[22] V. Hlukhyy, T. F. Fässler, *Z. Anorg. Allg. Chem.* **2010**, *636*, 100–107.
[23] L. Siggelkow, V. Hlukhyy, T. F. Fässler, *Z. Anorg. Allg. Chem.* **2010**, *636*, 1870–1879.
[24] V. Hlukhyy, N. Chumalo, V. Zaremba, T. F. Fässler, *Z. Anorg. Allg. Chem.* **2008**, *634*, 1249–1255.
[25] O. I. Bodak, E. I. Gladyshevskii, *Dopov. Akad. Nauk Ukr. RSR* **1968**, *30*, 944–947.
[26] V. Hlukhyy, S. Eck, T. F. Fässler, *Inorg. Chem.* **2006**, *45*, 7408–7416.
[27] V. Hlukhyy, T. F. Fässler, *Proc. of GDCh Jahrestagung*, Düsseldorf, Germany, **2005**, Mat020.
[28] Z. Ban, M. Sikirica, *Acta Crystallogr.* **1965**, *18*, 594–599.
[29] H. Pfisterer, K. Schubert, *Z. Metallkd.* **1950**, *41*, 358–367.
[30] C. H. Johansson, J. O. Linde, *Annalen Physik* **1925**, *78*, 439–460.
[31] Containing papers of a mathematical and physical character: A. J. Bradley, A. H. Jay, *Proc. Royal Soc. London Ser. A* **1932**, *136*, 210–232.
[32] U. Müller, *Anorganische Strukturchemie*, 5th ed., Teubner Verlag/GWV Fachverlage GmbH, Wiesbaden, Germany, **2006**.
[33] D. Berthebaud, A. P. Goncalves, O. Tougait, M. Potel, E. B. Lopes, H. Noel, *Chem. Mater.* **2007**, *19*, 3441–3447.
[34] F. Zürcher, S. Wengert, R. Nesper, *Inorg. Chem.* **1999**, *38*, 4567–4569.
[35] W. Rieger, E. Parthe, *Monatsh. Chem.* **1969**, *100*, 439–443.
[36] P. Villars, L. D. Calvert, *Pearson's Handbook of Crystallographic Data for Intermetallic Phases*, 2nd ed., ASM International, Materials Park, OH, **1991**.
[37] V. Hlukhyy, T. F. Fässler, *Z. Anorg. Allg. Chem.* **2008**, *634*, 2316–2322.
[38] V. Hlukhyy, A. Senyshyn, D. Trots, T. F. Fässler, *HASYLAB Ann. Rep.* **2007**, *1*, 1021–1022.
[39] K. H. Janzon, H. Schäfer, A. Weiss, *Z. Naturforsch., B: J. Chem. Sci.* **1968**, *23*, 1544–1544.
[40] E. Hellner, *Z. Anorg. Allg. Chem.* **1950**, *261*, 226–236.
[41] P. Eckerlin, E. Wolfel, *Z. Anorg. Allg. Chem.* **1955**, *280*, 321–331.
[42] V. Hlukhyy, L. Siggelkow, T. F. Fässler, manuscript in preparation, **2011**.
[43] STOE, *WinXPOW*, version 2.08, STOE & Cie GmbH, Darmstadt, Germany, **2003**.
[44] J. Rodriguez-Carvajal, *FullProf.2k*, version 3.2, Laboratoire Leon Brillouin (CEA-CNRS), France, **2005**.
[45] *CrysAlis RED*, *Scale3: ABSPACK*, version 1.171.33.41, Oxford Diffraction Poland Sp. z o. o., **2009**.
[46] *X-RED32*, *Data Reduction Program*, version 1.48, Stoe & Cie GmbH, Darmstadt, Germany, **2008**.
[47] *X-SHAPE*, *Crystal Optimization for Numerical Absorption Correction*, version 2.11, STOE & Cie GmbH, Darmstadt, Germany, **2008**.
[48] G. M. Sheldrick, *SHELXS-97*, *Program for the Determination of Crystal Structures*, University of Göttingen, Germany, **1997**.
[49] G. M. Sheldrick, *SHELXL-97*, *Program for Crystal Structure Refinement*, University of Göttingen, Germany, **1997**.
[50] L. M. Gelato, E. Parthe, *J. Appl. Crystallogr.* **1987**, *20*, 139–143.
[51] M. V. Schilfgarde, T. A. Paxton, O. Jepsen, O. K. Andersen, G. Krier, *The Stuttgart Tight-Binding LMTO-ASA*, version 4.7, Max-Planck-Institut für Festkörperforschung, Stuttgart, Germany, **1998**.
[52] U. V. Barth, L. Hedin, *J. Phys. C* **1972**, *5*, 1629–1642.
[53] O. Jepsen, O. K. Andersen, *Z. Phys. B* **1995**, *97*, 35–47.
[54] O. K. Andersen, O. Jepsen, *Phys. Rev. Lett.* **1984**, *53*, 2571–2574.
[55] R. Dronskowski, P. E. Blochl, *J. Phys. Chem.* **1993**, *97*, 8617–8624.
[56] A. D. Becke, K. E. Edgecombe, *J. Chem. Phys.* **1990**, *92*, 5397–5403.
[57] T. F. Fässler, *Chem. Soc. Rev.* **2003**, *32*, 80–86.
[58] A. Savin, R. Nesper, S. Wengert, T. F. Fässler, *Angew. Chem.* **1997**, *109*, 1892–1918; *Angew. Chem. Int. Ed. Engl.* **1997**, *36*, 1808–1832.

Received: March 31, 2011
Published Online: August 3, 2011

